Heterogeneous Catalysis Hot Paper

International Edition: DOI: 10.1002/anie.201902136
German Edition: DOI: 10.1002/ange.201902136

Atom-by-Atom Resolution of Structure–Function Relations over Low-Nuclearity Metal Catalysts

Evgeniya Vorobyeva, Edvin Fako, Zupeng Chen, Sean M. Collins, Duncan Johnstone, Paul A. Midgley, Roland Hauert, Olga V. Safonova, Gianvito Vilé, Núria López, Sharon Mitchell, and Javier Pérez-Ramírez**

Abstract: *Controlling the structure sensitivity of catalyzed reactions over metals is central to developing atom-efficient chemical processes. Approaching the minimum ensemble size, the properties enter a non-scalable regime in which each atom counts. Almost all trends in this ultra-small frontier derive from surface science approaches using model systems, because of both synthetic and analytical challenges. Exploiting the unique coordination chemistry of carbon nitride, we discriminate through experiments and simulations the interplay between the geometry, electronic structure, and reactivity of palladium atoms, dimers, and trimers. Catalytic tests evidence application-dependent requirements of the active ensemble. In the semi-hydrogenation of alkynes, the nuclearity primarily impacts activity, whereas the selectivity and stability are affected in Suzuki coupling. This powerful approach will provide practical insights into the design of heterogeneous catalysts comprising well-defined numbers of atoms.*

The dispersion of metals as tiny particles or clusters over high-surface-area hosts is common practice in heterogeneous catalysis.[1,2] It provides a means to tune the geometric and electronic characteristics compared to the bulk material while increasing the portion of atoms exposed for the adsorption and transformation of a substrate. The structure sensitivity of metal catalysts in different applications has primarily been investigated by controlling the size and/or shape of relatively large supported nanoparticles (> 1 nm).[3,4] In this range, size-dependent behavior can mainly be assigned to changes in the relative amounts or different surfaces and consequent distinctions in the electron densities around edge and defect sites. Moving to subnanometer dimensions alters these properties because of both increased electron confinement and interaction with the host material.[5] This non-scalable regime originates a non-linear variation of reactivity patterns that widens the applicability of metal catalysts. At the ultimate limit, the use of single-atom heterogeneous catalysts is rapidly expanding due to advances in their synthesis and characterization facilitated by their more readily distinguishable microscopic features.[6,7] While isolated atoms display attractive characteristics with respect to nanoparticles in some reactions,[8,9] they are not always the preferred structural unit.[4,10] In this regard, understanding the atom-by-atom behavior of low-nuclearity clusters is fundamental, but addressing this still presents numerous challenges.

Pioneering surface science approaches used model systems to derive trends with cluster size in reactions involving simple substrates, such as CO oxidation,[10,11] propane oxidative dehydrogenation,[12] O_2 reduction,[13] and propene epoxidation.[14] These works suggest that the addition or removal of a single atom can control the catalytic response.[15] However, the preservation of the nuclearity post-deposition and during application lacks direct evidences and is the major concern. Alternative synthetic strategies mainly involve the wet deposition of metal complexes of the desired number of atoms.[16–20] In this way, iridium dimers supported on Fe_2O_3[17] and WO_3[18] were shown to exhibit enhanced water photo-oxidation performance compared to Ir atoms or nanoparticles, by reducing the energy barrier for the third proton-coupled electron transfer step in the catalytic cycle. Similarly, Fe, Pd, and Ir dimers were immobilized on carbon nitride.[19] Only the iron-based catalysts were active in the targeted epoxidation of *trans*-stilbene and dimers yielded superior performance to atoms. In one of few studies on metal trimers, Ru_3 stabilized on nitrogen-doped carbon was found to efficiently catalyze the selective oxidation of alcohols.[20] Despite this progress, the mechanistic origin of the enhanced activity remains poorly understood. Furthermore, the lack of systematic assessment of the dynamics of the catalyst and its long-term stability under the reaction conditions is of major concern.

By merging advanced experimental and theoretical approaches including aberration-corrected scanning transmission electron microscopy (AC-STEM), X-ray photoelec-

[*] E. Vorobyeva, Dr. Z. Chen, Dr. G. Vilé, Dr. S. Mitchell, Prof. J. Pérez-Ramírez
Institute for Chemical and Bioengineering, Department of Chemistry and Applied Biosciences, ETH Zürich
Vladimir-Prelog-Weg 1, 8093 Zürich (Switzerland)
E-mail: msharon@chem.ethz.ch
jpr@chem.ethz.ch
E. Fako, Prof. N. López
Institute of Chemical Research of Catalonia and Barcelona Institute of Science and Technology
Av. Països Catalans 16, 43007 Tarragona (Spain)
Dr. S. M. Collins, Dr. D. Johnstone, Prof. P. A. Midgley
Department of Materials Science and Metallurgy, University of Cambridge
Cambridge CB3 0FS (UK)
Dr. R. Hauert
Empa, Swiss Federal Laboratories for Materials Science and Technology, Überlandstrasse 129, 8600 Dübendorf (Switzerland)
Dr. O. V. Safonova
Paul Scherrer Institute
5232 Villigen (Switzerland)
Supporting information and the ORCID identification number(s) for the author(s) of this article can be found under: https://doi.org/10.1002/anie.201902136.

tron spectroscopy (XPS), X-ray absorption spectroscopy (XAS), density functional theory (DFT), and Born–Oppenheimer molecular dynamics (BOMD), this work elucidates the structure of three catalysts with distinct nuclearity (Pd_x, $x = 1, 2, 3$) on an exfoliated carbon nitride (ECN) host. This enables rationalization of their catalytic behavior in the semi-hydrogenation of alkynes and Suzuki coupling, chemical transformations of increasing complexity. To achieve this, we exploit the multidentate coordination of the heteromacrocycles of carbon nitride (C_3N_4) to accommodate metal species of different nuclearity (Figure 1 a). Although attractive for comparative purposes, the controlled aggregation of Pd atoms via thermal treatment is unsuccessful (Figure S1 in the Supporting Information). Alternatively, the deposition of dimeric and trimeric palladium complexes appears a more promising strategy for the controlled introduction of low-nuclearity clusters on ECN without alteration of the carrier structure (Figure S2). Metal contents close to the targeted value of 0.5 wt % are achieved in all cases (Table S1) as well as complete decomposition of the precursor ligands (Figure S3).

AC-STEM imaging confirms the high metal dispersion in the Pd_x/ECN catalysts. Although features resembling dimers and trimers can be identified (Figure 1 b–d, Figure S4), several factors hamper the clear visualization of these metal ensembles, not least their multiple and varied orientations on the three-dimensional irregular structure of ECN (Supporting Information) and the dynamic connection between these orientations (see below).[21] To gain more quantitative insights, we adopted a statistical approach comparing the measured and theoretical (random dispersion) nearest neighbor (NN) distance distributions between Pd atoms.[22] As expected in the presence of isolated atoms these curves directly overlap in Pd_1/ECN (mean NN distance = 0.44 nm). In contrast, a progressive shortening of the NN distances with respect to the random distribution in both Pd_2/ECN (0.35 nm) and Pd_3/ECN (0.26 nm) agrees with a closer proximity of Pd centers, approaching typical values for a Pd–Pd bond. To avoid any effect of overlapping ensembles on the measured distribution, samples with lower Pd contents (0.1 wt %) were targeted to reduce the areal density of metal species, evidencing similar trends (Figure S5). The multidentate sites of the carbon nitride scaffold can accommodate Pd moieties with various coordination structures that are dynamically sampled (Supporting Movies 1–3).[23] Interestingly, the Pd–Pd

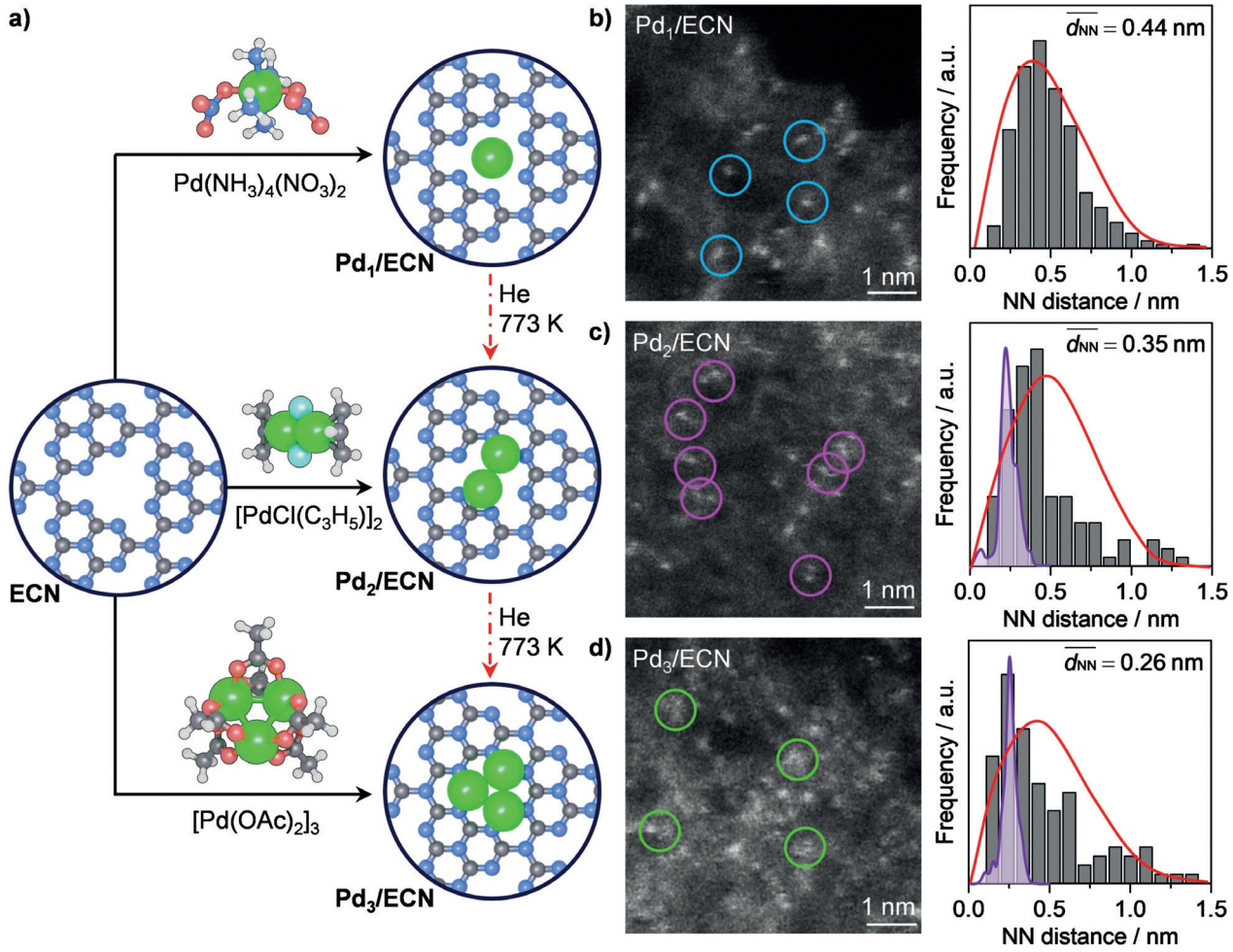

Figure 1. a) Approaches to prepare low-nuclearity Pd catalysts based on carbon nitride. Broken red arrows indicate unsuccessful routes. b)–d) AC-STEM images of the resulting catalysts with the measured (gray bars), predicted by BOMD (purple shaded curves), and theoretical random (red curves) NN distance distributions. Selected Pd atoms (blue circles), dimers (pink circles), and trimers (green circles) are identified.

distance distributions estimated by projection of the 3D structures simulated by BOMD on the *xy* plane closely match those derived by AC-STEM (Figure 1 b–d).

DFT calculations support the favorable stabilization of the dimers and trimers on ECN following removal of the ligand. The formation energies per Pd atom, $E_{form} = -3.47$, -0.92, and -1.37 eV for Pd_1/ECN, Pd_2/ECN, and Pd_3/ECN, respectively (Table S2), indicate a slightly weaker interaction for the metal dimers and trimers than for single atoms (Figure S6). The possible dissociation of dimers into isolated atoms cannot be completely excluded, while for the trimer this is less likely. Comparatively, both the agglomeration of single atoms to dimers and of dimers to trimers are unlikely (Table S3).

Previous studies have evidenced the cationic nature of Pd atoms isolated on ECN.[24,25] Similarly, analysis by XPS distinguishes two positively charged Pd species in the cases of Pd_2/ECN and Pd_3/ECN, which are tentatively assigned to Pd^{4+} (338.5 eV) and Pd^{2+} (336.9 eV) based on formal charges (Figure 2 a). Nevertheless, the Pd^{2+}:Pd^{4+} ratio varies from 0.56 (Pd_1/ECN) to 0.61 (Pd_2/ECN) to 0.93 (Pd_3/ECN), evidencing a reduced degree of oxidation with increasing nuclearity, which agrees with the predicted weaker interaction with the host. Notably, the signal of bulk metal at 335.0 eV was not observed in any sample. The XPS shifts simulated along the BOMD trajectories (Figure 2 b) show that Pd atoms localized close to the surface are less oxidized (Pd^{2+}-like) than those residing in the subsurface (Pd^{4+}-like) of the C_3N_4 structure.

To gain further insight into the coordination environment of the Pd species, we investigated the catalysts by XAS (Figure 2 c, Figure S7). The fitted results (Table S4) of the extended absorption X-ray fine structure (EXAFS) at the Pd K-edge reveal that the strong signal at 1.7 Å primarily originates from the first coordination neighbor (N or O), with an associated coordination distance of 2.019 Å. A similar Pd–N interaction appears in the radial distribution functions (RDF, Figure 2 d) of Pd calculated by BOMD. For Pd_1/ECN, BOMD shows that the first coordination sphere is formed by N, but full bonding to all 6 N in the cavity has low probability. This reduces the average N (N or O for EXAFS) coordination number of Pd to 3.4 ± 0.3 (EXAFS) and 4.3 ± 0.9 (BOMD, Table S5). Distortions of the scaffold and the movement of Pd within the cavity yield a non-equidistant first coordination sphere even if comprised solely of nitrogen (Figure S8). For Pd_2/ECN and Pd_3/ECN the less pronounced interaction with the scaffold lowers the average Pd–N coordination number to $2.5 \pm 0.3/3.8 \pm 0.8$ and $2.8 \pm 0.3/2.3 \pm 0.7$ for EXAFS/BOMD, respectively, due to the presence of Pd atoms in the first coordination sphere (Figure S5, Figure S9). A small interaction between Pd and C atoms is also observed by BOMD deriving from ensembles in subsurface positions. Notably, no strong signal associated with Pd–Pd bonding is visible in any spectra. The reason for this becomes apparent when inspecting the radial distribution functions extracted from the BOMD trajectories. Due to the low nuclearity and wide Pd–Pd bond length variation (Figure 1 b–d), the dominant Pd-scaffold interactions strongly affect the metal-metal peaks. Additionally, the fact that scattering signals generated by different Pd–Pd couples destructively interfere because they are not in phase due to very broad bond-length distribution render their detection by EXAFS almost impossible. CO adsorption was studied as a method to discriminate the

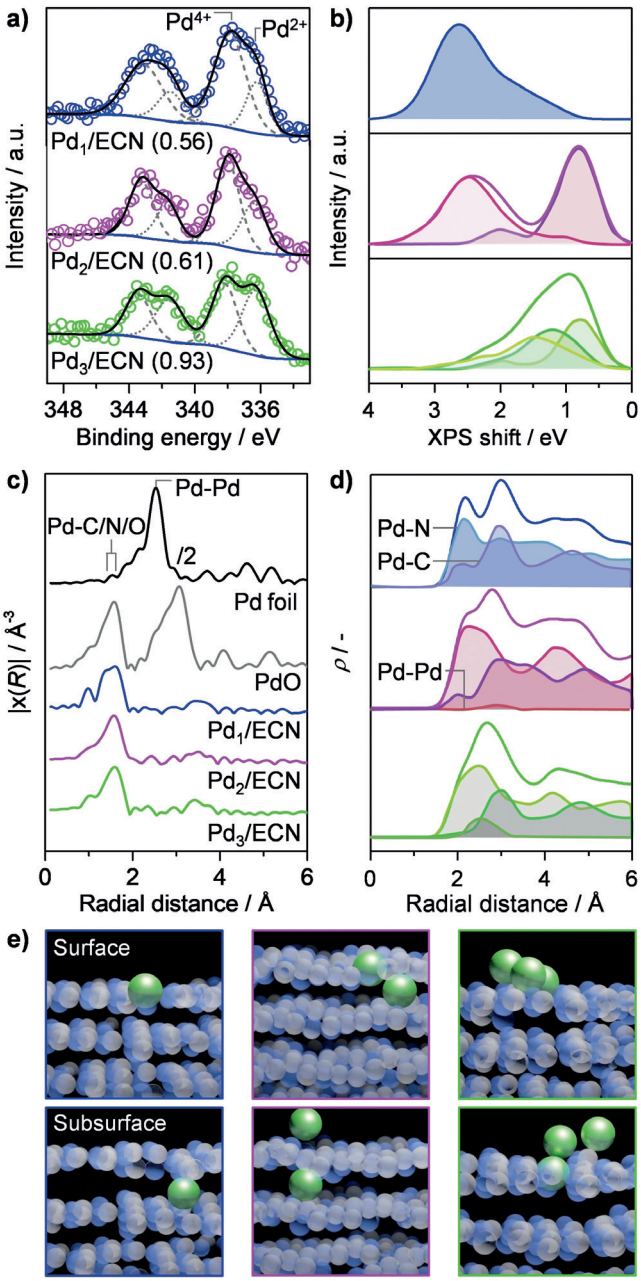

Figure 2. a) Measured and b) simulated Pd 3d core level XPS spectra of the Pd_x/ECN catalysts. In (a), black lines show the fits of the raw data (open symbols), gray lines deconvolute the components tentatively assigned to Pd^{4+} (dashed) and Pd^{2+} (dotted) species, and blue lines show the background. The Pd^{2+}:Pd^{4+} ratios are indicated in parenthesis. In (b), colored lines represent each Pd atom in the ensemble. c) Normalized k^2-weighted Fourier Transform of the EXAFS function of the Pd_x/ECN catalysts and reference compounds. d) Sum of the radial distribution functions over all the structures generated during the BOMD runs, with the Pd atoms as the reference for Pd_x/ECN. e) Snapshots from the BOMD simulations (Supporting Movies 1–3) illustrating distinct possible surface and subsurface configurations of metal ensembles. Green Pd, pale blue N, and grey C.

uniformity of the metal speciation, but it was not possible to detect by pulse chemisorption measurements or IR spectroscopy (Figure S10). This relates to the fact that the Pd ensembles coexist in subsurface configurations (Figure 2e) in which the electron density of the scaffold shields Pd preventing CO adsorption.

All catalysts convert 2-methyl-3-butyn-2-ol into 2-methyl-3-buten-2-ol with high stability and full chemoselectivity (100%) under the investigated conditions. Consistently, the oxidation state, metal content, and atomic dispersion are preserved after five catalytic runs (Figure S11). However, significant differences are evident in terms of activity versus nuclearity, with Pd_3/ECN exhibiting a reaction rate (0.73×10^3 $mol_{-ene}\, mol_{Pd}^{-1}\, h^{-1}$) 3.8 times higher than that over Pd_2/ECN and Pd_1/ECN (Figure 3a, Figure S12). We have explored the effect of the nuclearity when all the atoms are exposed on the surface. The superior performance of Pd_3/ECN originates from the barrierless, homolytic H_2 activation path on hcp-like sites. This requires a minimum ensemble of three atoms and leaves a bridge site available for adsorbing the alkyne, resembling the Pd(111) surface.[26] In contrast, Pd_1/ECN and Pd_2/ECN exhibit higher barriers for this step as the mechanism follows a heterolytic route involving the transfer of a H atom to the scaffold (Figure 3b). This opens the coordination sphere of Pd and allows the triple-bond adsorption and subsequent H transfer. The second H is then recovered to the metal center, prior to the hydrogenation to the alkene and ready desorption of this product. Slightly enhanced performance of the dimers could be expected due to the existence of a bridge site, leading to more exothermic (−0.81 and −1.16 eV, Pd_1/ECN and Pd_2/ECN, respectively) hydrogen activation than over single atoms. However, this is only possible when both atoms are located in surface positions and dimers mostly populate a configuration with one subsurface atom (Supporting Movie 2). This issue is not encountered for Pd_3/ECN because the subsurface configurations are less favorable for the trimers (Figure S13). This nuclearity trend was generalized to the transformation of diverse linear and branched alkynes (Figure 3c).

Opposite nuclearity effects are observed in the continuous Suzuki coupling of bromobenzene with phenylboronic acid pinacol ester (Table 1). Pd_1/ECN exhibits the highest rate of biphenyl formation, and was recently shown to surpass state-of-the-art homogenous and heterogeneous catalysts in this

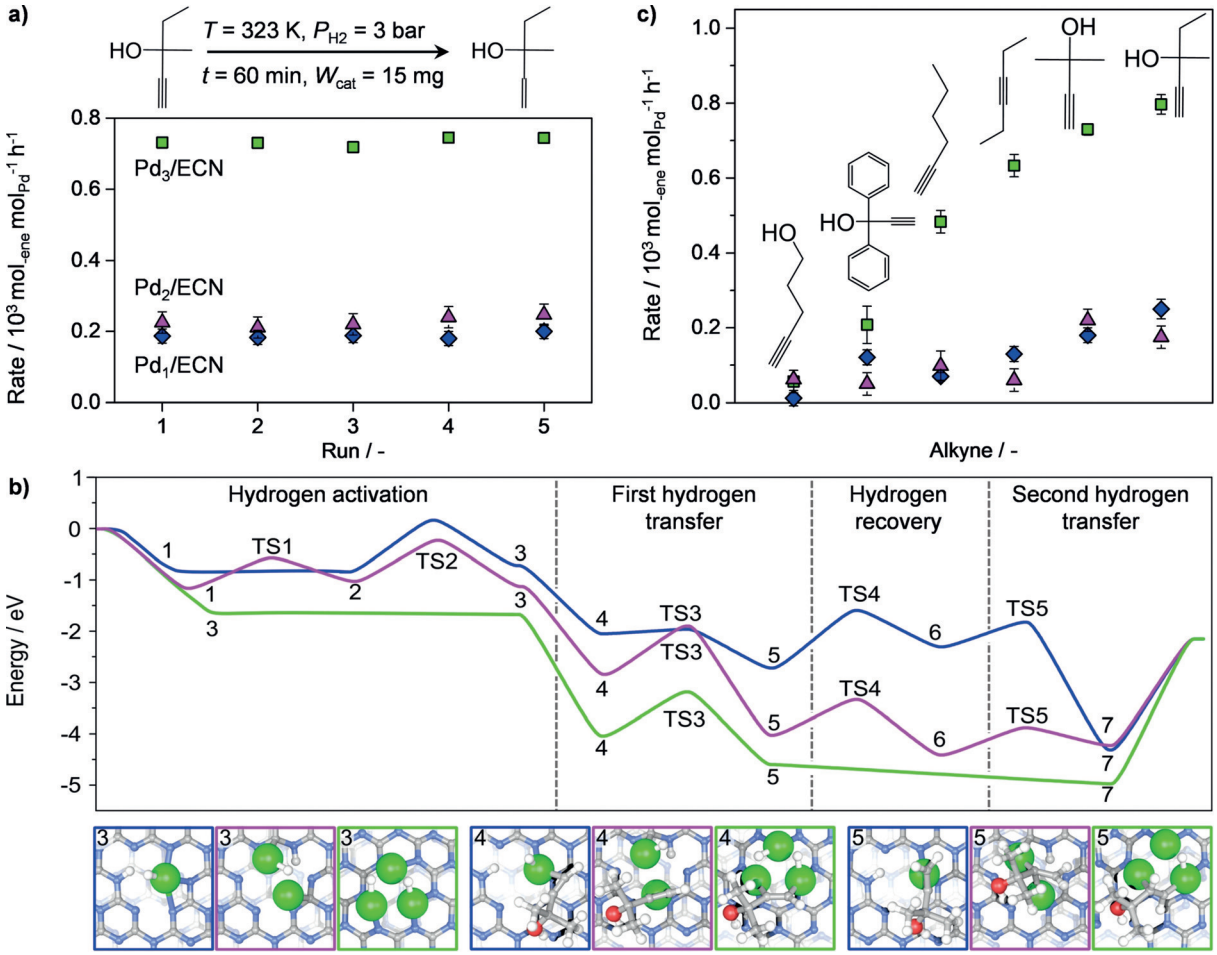

Figure 3. a) Variation in the rates of 2-methyl-3-buten-2-ol formation in the hydrogenation of 2-methyl-3-butyn-2-ol (depicted) over five sequential runs and b) the calculated reaction paths over the surface configurations (with all atoms at the surface) of the Pd ensembles in Pd_x/ECN. Green Pd, gray C, blue N, red O, and white H atoms. TS = transition state. c) Rates of alkene formation in the hydrogenation of distinct functionalized alkynes (illustrated). The color code for data points in (a) applies to (b) and (c).

Table 1: Performance in the continuous reaction of bromobenzene with phenylboronic acid pinacol ester (depicted).

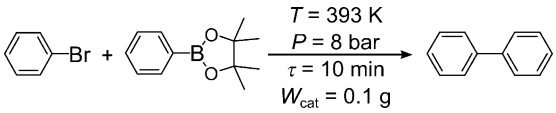

Sample[a]	Pd[a] [wt%]	X[b] [%]	S[c] [%]	r[d] [mol mol^{-1} h^{-1}]
Pd_1/ECN	0.57	54	89	538
Pd_2/ECN	0.46	79	49	516
Pd_3/ECN	0.46	19	79	208

[a] ICP-OES. [b] Conversion and [c] selectivity determined by high-performance liquid chromatography. [d] Rate of biphenyl formation per mole of Pd.

reaction.[23] A similar rate is evidenced over Pd_2/ECN, but this catalyst is found to be more active and less selective, while Pd_3/ECN displays only limited conversion. Analysis of the used catalysts confirms a high stability of single atoms, but reveals metal losses (Table S1) and the formation of nanoparticles in the case of dimers and trimers (Figure S14). The different performance originates in the first oxidative addition of bromobenzene, and relate to a nuclearity-dependent chemoselectivity (Figure 4). Single atoms tend to activate the Br-phenyl bond and provide the adaptive coordination environment for the following transmetallation and reductive elimination steps. However, on dimers and especially trimers the aromatic ring adsorbs to the nanocluster strongly, poisoning the active site, and weakening the interaction of the metal cluster to the carbon nitride scaffold. This induces the extraction of Pd from the anchoring site and consequent aggregation.

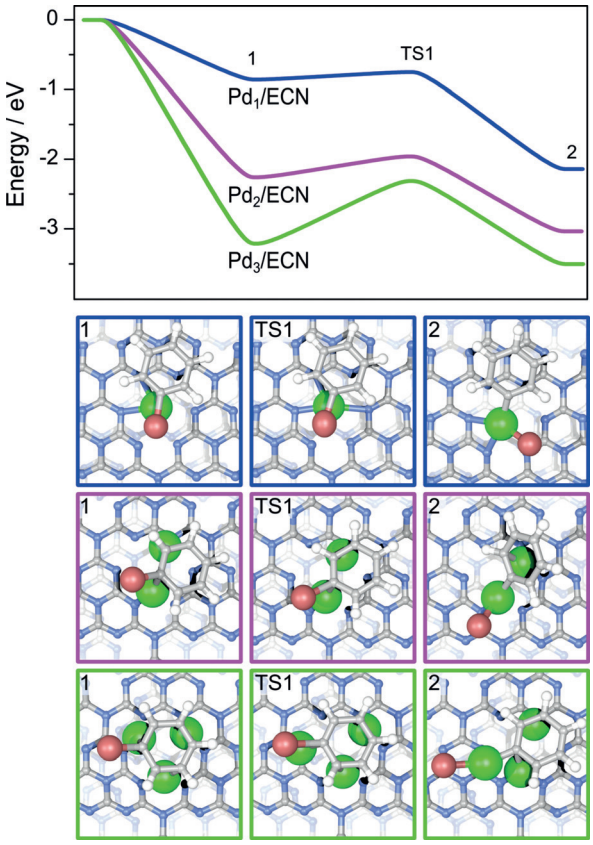

Figure 4. Reaction paths of the coupling of bromobenzene with phenylboronic acid pinacol ester over the surface configurations of the Pd ensembles in Pd_x/ECN. Atom coloring as in Figure 3, Br in dark red.

In conclusion, by exploiting the versatile coordination chemistry of carbon nitride, palladium atoms, dimers, and trimers were anchored on this host enabling comparison of their structure and reactivity. Simulations of the dynamic structure of the low-nuclearity species provided essential insights to interpret the experimental observations. Catalytic tests in alkyne semi-hydrogenation and Suzuki coupling revealed opposite application-dependent nuclearity effects. Pd trimers were more active in the selective hydrogenation of various functionalized alkynes, which was linked to the reduced hydrogen activation barrier with respect to single atoms and dimers. In contrast, Pd single atoms surpass ensembles in Suzuki coupling exhibiting distinct chemoselectivity to the dimers and trimers, which also ensured higher stability. While all evidence points towards the successful stabilization of the desired ensembles, establishing the uniformity of the metal speciation remains an important challenge that deserves urgent attention.

Experimental Section

Full details on the catalyst synthesis, characterization, testing, and calculations are given in the Supporting Information. Pd_1/ECN was prepared following a previously reported recipe.[23] Pd_2/ECN and Pd_3/ECN were obtained by microwave-assisted deposition of the corresponding precursors (allyl palladium chloride dimer or palladium acetate trimer) in toluene onto ECN. The resulting solids were collected by filtration, washed, dried, and subsequently thermally-treated to ensure removal of the ligands. The structure and properties of the Pd species of different nuclearity were studied in depth by AC-STEM, XPS, XAS, DFT (PBE + D3), and BOMD. Catalytic tests in alkyne semi-hydrogenation and Suzuki coupling were conducted in batch continuous mode, respectively.

Acknowledgements

We are grateful to the SNSF (200021-169679, E.V., Z.C., S.M., J.P.-R.), the Severo Ochoa Excellence program (SEV-2013-0319, E.F.), the EPSRC (Grant no. EP/R008779/1, P.A.M.), and the Henslow Research Fellowship of Girton College, Cambridge (S.M.C.) for funding this work. We thank ScopeM and BSC-RES for access to facilities, and Diamond Light Source for access and support in the use of the electron Physical Science Imaging Centre (EM17997).

Conflict of interest

The authors declare no conflict of interest.

Keywords: C–C coupling · heterogeneous catalysis · hydrogenation · metal clusters · structure–activity relationships

How to cite: *Angew. Chem. Int. Ed.* **2019**, *58*, 8724 – 8729
Angew. Chem. **2019**, *131*, 8816 – 8821

[1] A. T. Bell, *Science* **2003**, *299*, 1688 – 1691.
[2] R. J. White, R. Luque, V. L. Budarin, J. H. Clark, D. J. Macquarrie, *Chem. Soc. Rev.* **2009**, *38*, 481 – 494.
[3] S. Cao, F. Tao, Y. Tang, Y. Li, J. Yu, *Chem. Soc. Rev.* **2016**, *45*, 4747 – 4765.
[4] L. Liu, A. Corma, *Chem. Rev.* **2018**, *118*, 4981 – 5079.
[5] X.-F. Yang, A. Wang, B. Qiao, J. Li, J. Liu, T. Zhang, *Acc. Chem. Res.* **2013**, *46*, 1740 – 1748.
[6] A. Wang, J. Li, T. Zhang, *Nat. Rev. Chem.* **2018**, *2*, 65 – 81.
[7] Q. Fu, H. Saltsburg, M. Flytzani-Stephanopoulos, *Science* **2003**, *301*, 935 – 938.
[8] G. Kyriakou, M. B. Boucher, A. D. Jewell, E. A. Lewis, T. J. Lawton, A. E. Baber, H. L. Tierny, M. Flytzani-Stephanopoulos, E. C. H. Sykes, *Science* **2012**, *335*, 1209 – 1212.
[9] S. Mitchell, E. Vorobyeva, J. Pérez-Ramírez, *Angew. Chem. Int. Ed.* **2018**, *57*, 15316 – 15329; *Angew. Chem.* **2018**, *130*, 15538 – 15552.
[10] A. Sanchez, S. Abbet, U. Heiz, W.-D. Schneider, H. Häkkinen, R. N. Barnett, U. Landman, *J. Phys. Chem. A* **1999**, *103*, 9573 – 9578.
[11] B. Yoon, H. Häkkinen, U. Landman, A. S. Wörz, J.-M. Antonietti, S. Abbet, K. Judai, U. Heiz, *Science* **2005**, *307*, 403 – 407.
[12] S. Vajda, et al., *Nat. Mater.* **2009**, *8*, 213 – 216.
[13] M. Nesselberger, et al., *Nat. Mater.* **2013**, *12*, 919 – 924.
[14] Y. Lei, et al., *Science* **2010**, *328*, 224 – 228.
[15] E. C. Tyo, S. Vajda, *Nat. Nanotechnol.* **2015**, *10*, 577 – 588.
[16] T. Imaoka, Y. Akanuma, N. Haruta, S. Tsuchiya, K. Ishihara, T. Okayasu, W.-J. Chun, M. Takahashi, k. Yamamoto, *Nat. Commun.* **2017**, *8*, 688.
[17] Y. Zhao, et al., *Proc. Natl. Acad. Sci. USA* **2018**, *115*, 2902 – 2907.
[18] Y. Zhao, et al., *ACS Cent. Sci.* **2018**, *4*, 1166 – 1172.
[19] S. Tian, et al., *Nat. Commun.* **2018**, *9*, 2353.
[20] S. Ji, et al., *J. Am. Chem. Soc.* **2017**, *139*, 9795 – 9798.
[21] M. Utlaut, *Phys. Rev. B* **1980**, *22*, 4650 – 4660.
[22] Z. Chen, et al., *Adv. Funct. Mater.* **2017**, *27*, 1605785.
[23] Z. Chen, et al., *Nat. Nanotechnol.* **2018**, *13*, 702 – 707.
[24] E. Vorobyeva, et al., *J. Mater. Chem. A* **2017**, *5*, 16393 – 16403.
[25] Z. Chen, et al., *Natl. Sci. Rev.* **2018**, *5*, 642 – 652.
[26] D. Albani, M. Shahrokhi, Z. Chen, S. Mitchell, R. Hauert, N. López, J. Pérez-Ramírez, *Nat. Commun.* **2018**, *9*, 2634.

Manuscript received: February 18, 2019
Accepted manuscript online: May 2, 2019
Version of record online: May 17, 2019

